Appendix 5

Titus Kuehne, MD
Steffen Weiss, PhD
Florian Brinkert, MD
Jochen Weil, MD
Sevim Yilmaz, MD
Boris Schmitt, MD
Peter Ewert, MD
Peter Lange, MD
Matthias Gutberlet, MD

Index terms:
Animals
Arteries, grafts and prostheses
Catheters and catheterization, technology
Magnetic resonance (MR), guidance, 56.1294, 94.1294
Stents and prostheses

Published online before print
10.1148/radiol.2333031710
Radiology 2004; 233:774–780

Abbreviations:
FFE = fast field echo
RC = resonant circuit
SDS = stent delivery system
SI = signal intensity
3D = three-dimensional

[1] From the Departments of Congenital Heart Disease and Pediatric Cardiology, German Heart Institute, Augustenburger Platz 1, Berlin 13037, Germany (T.K., S.Y., B.S., P.E., P.L.); Philips Research Laboratories, Hamburg, Germany (S.W.); Department of Pediatric Cardiology, University Hospital Eppendorf, Hamburg, Germany (F.B., J.W.); and Department of Diagnostic Radiology and Nuclear Medicine, Charité, Humboldt University, Berlin, Germany (M.G.). Received October 28, 2003; revision requested January 16, 2004; revision received March 11; accepted April 1. Supported in part by the German Bundesministerium für Bildung und Forschung and the Deutsche Forschungsgemeinschaft. **Address correspondence to** T.K. (e-mail: *titus.kuehne@dhzb.de*).

Author contributions:
Guarantors of integrity of entire study, T.K., F.B., M.G., S.W.; study concepts and design, T.K., F.B., S.W.; literature research, T.K., F.B., J.W., S.Y., B.S., P.E.; experimental studies, T.K., F.B., S.Y., B.S., P.E., M.G., S.W.; data acquisition, T.K., M.G., B.S., S.W.; data analysis/interpretation, T.K., F.B., S.W.; statistical analysis, T.K., F.B.; manuscript preparation, T.K.; manuscript definition of intellectual content, T.K., F.B., J.W., M.G., B.S., P.E., S.W.; manuscript editing, revision/review, and final version approval, all authors

Catheter Visualization with Resonant Markers at MR Imaging–guided Deployment of Endovascular Stents in Swine[1]

PURPOSE: To evaluate resonant circuits as markers for magnetic resonance (MR) imaging–guided placement of nitinol stents.

MATERIALS AND METHODS: The study was approved by the institutional animal research committee and complied with National Institutes of Health guidelines for care and use of laboratory animals. Resonant circuits similar to catheter markers used at conventional angiography were placed proximally and distally to a nitinol stent in a stent delivery system. Resonant circuits were tested in vitro and in vivo for signal intensity levels that would enable visualization during MR imaging–guided stent deployment. Experiments were conducted by using real-time imaging with a 1.5-T unit. Stents ($n = 9$) were deployed in the vena cava ($n = 2$), abdominal aorta ($n = 2$), isthmus of the aorta ($n = 2$), and carotid ($n = 2$) and iliac ($n = 1$) arteries in five pigs. After intervention, the site of the stent was investigated with balanced fast field-echo MR imaging and contrast material–enhanced MR angiography. Blood flow velocities were measured in the stent lumen and next to the stent with velocity-encoded cine MR imaging. Level of agreement was determined with Bland-Altman analysis.

RESULTS: During all interventions, resonant circuits provided highly visible MR signal that allowed fast and reliable visualization of the stent delivery system. Borders of loaded stents were clearly marked, which allowed precise stent placement in all experiments. Balanced fast field-echo MR imaging and contrast-enhanced MR angiography provided information about immediate postintervention position. Positions depicted on MR images were found accurate at postmortem examination. Results of Bland-Altman analysis showed good agreement between blood flow velocities measured in and next to the stent lumen, with a mean difference of −9 cm/sec ± 5 (standard deviation).

CONCLUSION: Resonant circuits are well suited for use at deployment of endovascular stents.

Magnetic resonance (MR) imaging–guided endovascular intervention is a rapidly developing field of basic research and preliminary clinical experience. MR imagers have been recently modified for use in interventional procedures. At the same time, the technologic development of MR-compatible devices is proceeding at a fast pace. Several groups (1–3) have reported the feasibility of endovascular procedures performed with MR imaging guidance.

MR imaging research with catheter tracking has resulted in a number of methods for active and passive tracking. Active tracking is accomplished by incorporating a small receiver coil into the tip of a device (4,5). Results of several studies, however, have shown that the use of active catheter tracking techniques may be hazardous to the patient (6–8).

Passive tracking of endovascular catheters is based on the integration of magnetic susceptibility markers (9,10) or contrast agents (11) into the device. The use of this technique, however, often results in insufficient contrast between the interventional instrument and the anatomy that surrounds it (1–3). In addition, passive tracking techniques do not deliver coordinates, as is required for fast and automated device localization.

The use of wireless resonant circuits (RCs) as fiducial markers of endovascular catheters has been proposed as an alternative to conventional passive and active methods for catheter tracking (12–14). The main advantages of RCs are that they *(a)* produce an intense local signal intensity enhancement, which is readily perceptible to the observer at any catheter orientation (14), *(b)* do not contain any elongated conductors and can be constructed such that no physiologically relevant heating occurs (13), and *(c)* allow for automated tip detection and section tracking (13).

RCs, if tuned to the Larmor frequency, substantially enhance the excitation angle in and adjacent to the fiducial coil and locally increase the sensitivity of the receive coil. Accurate fine-tuning of the RC is essential for its appropriate function. However, tuning is problematic when RCs are mounted on interventional instruments such as stent delivery systems (SDSs). SDSs are composed of various materials and include multiple layers of polyesters, as well as the loaded metallic stents. In addition, during intervention, various kinds of guidewires are alternately inserted into the lumen of the SDS. All these materials can either diminish the quality factor of the RC or electromagnetically interact with the RC and in turn influence its tuning condition.

The aim of this study was to evaluate RCs as markers on endovascular catheters for MR imaging–guided placement of nitinol stents.

MATERIALS AND METHODS

Stents and SDSs

Self-expanding nitinol stents (Flexx; Angiomed, Karlsruhe, Germany) with a diameter of 10 mm and a length of 30 mm were used. The nitinol stents consist of a paramagnetic metal alloy composed of 50% titanium and 50% nickel (15). Stents were front-loaded into a custom-made 6-F SDS that comprises an outer and an inner catheter. The outer catheter is made of polyurethane and has a material thickness of 0.4 mm. The inner catheter is made of polyester and provides a working lumen with a diameter of 0.035 inch. Stent delivery is achieved by pulling back the outer catheter over the front-loaded stent while a small polyester plunger at the tip of the inner catheter holds the stent in place during its expansion.

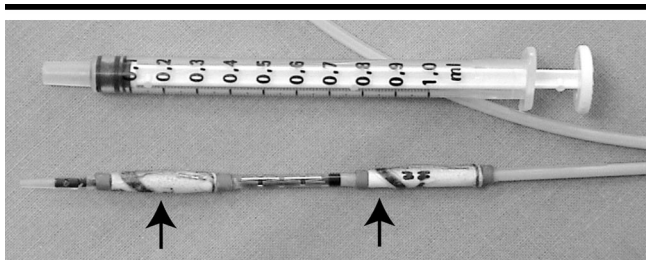

Figure 1. SDS with RCs (arrows) positioned at the distal and proximal ends of the loaded stent.

Resonant Circuits

RCs were coils constructed of thin copper wire and tuned to the Larmor frequency at 1.5 T. Tuning was achieved with multilayered ceramic capacitors with a capacity of 10–24 pF and a housing that measured 0.25 × 0.25 × 0.50 mm (Philips, Eindhoven, the Netherlands). Each RC coil consisted of between eight and 10 revolutions of 0.12-mm insulated copper wire. Coils were wound diagonally around the SDS at an angle of 45° to the long axis of the SDS (Fig 1).

RCs were glued to the outer catheter of the SDS and were positioned directly adjacent to the distal and proximal margins of the loaded stent (Fig 1). For the experiments, two different sets of RCs were constructed. The first set consisted of single RCs, whereas the second set comprised a pair of decoupled RCs. For decoupling, two individually tuned RCs were superimposed and oriented perpendicular to each other (14). The MR signal in catheters equipped with a pair of decoupled RCs is largely independent of catheter orientation with regard to the B_0 field direction, whereas the signal in catheters with single RCs is not (14).

While submerged in isotonic saline solution, RCs were tuned to 63.87 MHz with a network analyzer used in S-11 mode. Tuning was performed while a 0.035-inch nitinol guidewire (Microvena, White Bear Lake, Minn) was inserted through the working lumen of the SDS. For fine-tuning, a flexible coaxial cable (Precision Interconnect, Wilsonville, Ore) was connected to the capacitor, in parallel with the guidewire and with an open end. The coaxial cable yields an electric capacity of 0.94 pF/cm at 63.87 MHz. Fine-tuning was realized by shortening the coaxial cable stepwise to an average length of 7 mm ± 2. After tuning, RCs were coated with polyurethane. In their entirety, the RCs (including copper coils, capacitor, coaxial cable, and coating) had an average thickness of 1.8 mm ± 0.5. The outer diameter of the SDS with the RCs was 7.5 F. The quality factor of the RCs measured with the network analyzer in saline solution was 42 ± 10.

MR Imaging

All experiments were performed with a short-bore 1.5-T MR imager (Intera; Philips Medical Systems, Best, the Netherlands) by using a phased-array surface coil. In vitro measurements and MR guidance of interventional procedures were based on an interactive real-time steady-state free precession sequence. Imaging parameters were as follows: repetition time msec/echo time msec, 2.9/1.6; variable flip angle, 5° or 45°; variable section thickness, 8–10 mm; variable field of view, 200–350 mm; reconstruction field of view, 80%; matrix, 128 × 128; and cartesian k-space sampling. The acquisition rate was 8 frames per second, and the online reconstruction and display rate was 195 frames per second.

Preinterventional assessment of the targeted vasculature and postinterventional evaluation of stent position were performed with both balanced fast field-echo (FFE) MR imaging and contrast material–enhanced three-dimensional (3D) MR angiography. Imaging parameters for the balanced FFE sequence were as follows: 2.7/1.4, flip angle of 50°, section thickness of 8 mm, field of view of 200–350 mm, and matrix of 256 × 256. Imaging parameters for 3D MR angiography were 5.2/1.6, flip angle of 35°, section thickness of 1.6 mm, field of view of 350–400 mm, and matrix of 512 × 512. During

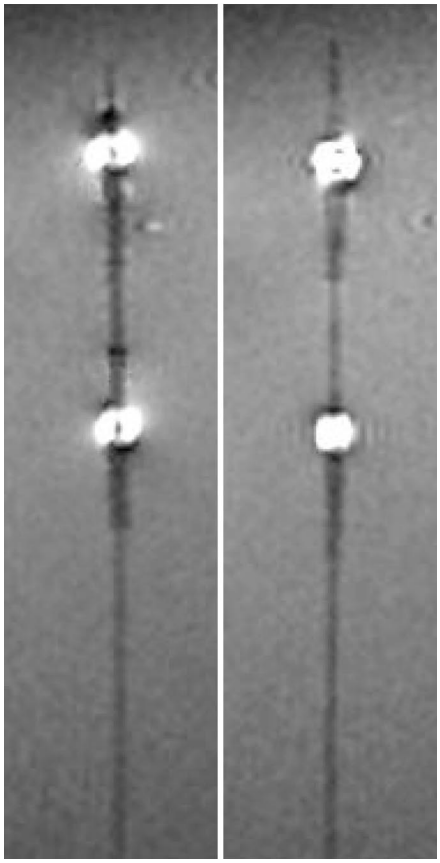

Figure 2. MR images acquired with interactive steady-state free precession (2.9/1.6; flip angle, 45°; section thickness, 8 mm; acquisition frame rate, 8 per second; field of view, 280 mm; matrix, 128 × 128) show SDS with RCs in saline bath. Note the intense signal of the RCs before (left) and after (right) delivery of the nitinol stent.

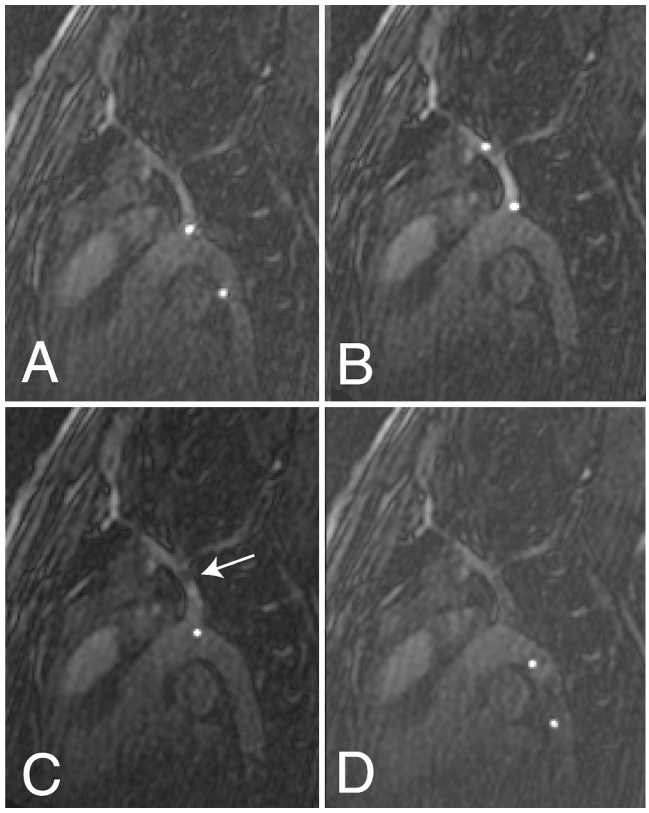

Figure 3. Parasagittal interactive steady-state free precession (2.9/1.6; flip angle, 5°; section thickness, 8 mm; acquisition frame rate, 8 per second; field of view, 280 mm; matrix, 128 × 128) MR images of the thoracic aorta, carotid artery, and SDS with single RCs show good contrast between SI of RCs and SI of background anatomy achieved with flip angle of 5°. *A,* Advancement of the SDS through the aortic arch. *B,* SDS in the carotid artery immediately before stent delivery. *C,* Release of the nitinol stent accompanied by detuning of the distal RC (arrow). *D,* Retraction of the SDS into the descending aorta.

MR angiography, gadopentetate dimeglumine (Magnevist; Schering, Berlin, Germany) at a dose of 0.2 mmol of gadolinium per kilogram body weight was injected intravenously at a rate of 4 mL/sec.

Velocity-encoded cine MR imaging was used for measurement of blood flow velocities in the stent lumen and adjacent to the stent immediately after intervention. Imaging parameters for velocity-encoded cine MR imaging (16) were as follows: 16/9, flip angle of 15°, field of view of 200–350 mm, reconstruction field of view of 50%, matrix of 256 × 256, section thickness of 8 mm, retrospective gating, 20 phases, and maximum limit of 200 cm/sec for velocity encoding.

In Vitro Experiments

A total of 12 SDSs were tested in vitro: Six were fitted with single RCs, and six, with a pair of decoupled RCs. All SDSs were immersed in a saline bath containing gadopentetate dimeglumine with a gadolinium concentration of 2.5 mmol/L (T1 = 360 msec, T2 = 280 msec). Signal intensity (SI) of the RCs was measured at flip angles of 45° and 5° by using interactive real-time MR imaging with a steady-state free precession sequence. Measurements were made with the SDSs aligned parallel to the B_0 field and at angles of 10°, 20°, 30°, 40°, 50°, 60°, 70°, 80°, and 90° to the B_0 field. SI was determined before and after release of the stent. During SI measurements, the lumen of the SDS was filled with saline solution. Further separate SI measurements were performed with the saline solution–filled lumen of the SDS alternately containing *(a)* a 0.035-inch nitinol guidewire and *(b)* a custom-made 0.035-inch polyester guidewire. SI was measured in an area of 4 pixels at the site of the RCs by three independent observers (T.K., F.B., S.W.).

In Vivo Experiments

All procedures were performed in accordance with the National Institutes of Health guidelines for care and use of laboratory animals and with the approval of the committee of animal research at our institution.

In five pigs (weight range, 18–28 kg), nine endovascular nitinol stents were deployed with MR imaging guidance. The animals were given an intramuscular injection of a mixture of telazol, ketamine, and xylazine at a dose of 0.025 mg/kg for induction of anesthesia, and 2% isoflurane was administered for maintenance of general anesthesia. Monitoring of vital parameters included electrocardiography and measurement of oxygen saturation. Vascular access was gained with the Seldinger technique in the iliac artery and vein and in the carotid artery. The animals were moved into the MR imag-

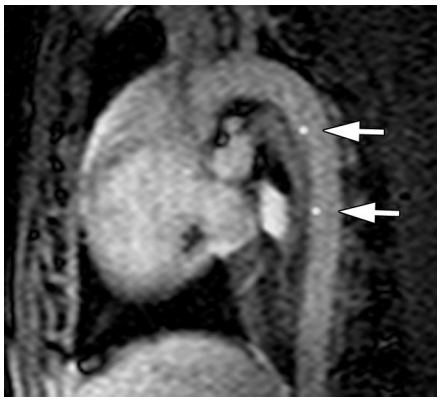

Figure 4. Parasagittal interactive steady-state free precession (2.9/1.6; flip angle, 45°; section thickness, 8 mm; acquisition frame rate, 8 per second; field of view, 280 mm; matrix, 128 × 128) MR image of the thoracic aorta and SDS with single RCs (arrows).

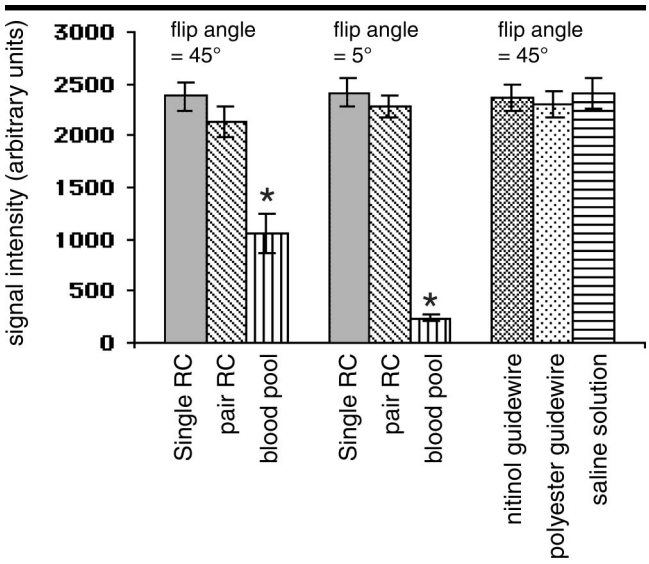

Figure 5. Bar graph shows in vivo SI measurements with two different flip angles over 4 pixels at the sites of single RCs and paired decoupled RCs and in blood within the vessel near the RC. Only SI of the blood pool (*) decreased significantly when the flip angle was changed from 45° to 5° ($P < .001$). No significant difference was found between SI measurements with the SDS lumen containing saline solution alone, saline solution and a nitinol guidewire, or saline solution and a polyester guidewire.

ing unit after this preparation in the animal care facilities. The targeted vasculature was investigated with balanced FFE and 3D MR angiographic pulse sequences. The SDS then was advanced through the sheath into the desired position during MR imaging with steady-state free precession for real-time interactive guidance.

Nitinol stents were deployed in one pig in each of the following locations: the inferior vena cava below the insertion of the renal veins (two stents), the abdominal aorta below the origin of the renal arteries (two stents), the isthmus of the aorta (two stents), the origin of the left common carotid artery at the aortic arch (two stents), and the common iliac artery distal to the bifurcation (one stent).

During intervention, SI was measured over 4 pixels at the site of the RCs and in the vessel lumen in the vicinity of the RCs with interactive real-time steady-state free precession imaging. Measurements were made at flip angles of 45° and 5°. For interventions in the vena cava and the aorta, SDSs with single RCs were used, because during these procedures the SDS is aligned parallel to the B_0 field. For interventions in the carotid and iliac arteries, SDSs with a pair of decoupled RCs were used. During these procedures, the SDS is oriented at different angles to the B_0 field as it is advanced from the aorta into the carotid or iliac artery. SI of the RCs was determined within the aorta, the vena cava, and the carotid and iliac arteries. SI was measured before and after stent delivery. Finally, SI in six SDSs (three with single RCs and three with a pair of decoupled RCs) was measured while the lumen of the SDS was *(a)* filled with saline solution, *(b)* filled with saline solution and holding a 0.035-inch nitinol guidewire, and *(c)* filled with saline solution and holding a 0.035-inch polyester guidewire. All measurements were repeated three times.

After intervention, the site of the stent was investigated with balanced FFE imaging and 3D MR angiography to determine the accuracy of deployment. Finally, peak flow velocities were measured in the stent lumen and distal or proximal to the stent with velocity-encoded cine MR imaging. Velocity measurements were performed twice at each site. All procedures were analyzed independently by each of three investigators (T.K., F.B., P.E.).

Autopsy of Animals

After completion of the study, the animals were euthanized with intravenous sodium pentobarbital (200 mg/kg). The inferior vena cava, aorta, and carotid and iliac arteries were dissected, and the position of the stent was determined with consensus by five authors (T.K., F.B., P.E., B.S., S.Y.).

Statistical Analysis

A paired Student *t* test was used to compare SI measured for the same type of RC at different orientations to the B_0 field and in different conditions (with and without use of guidewires and before and after stent delivery). An unpaired Student *t* test was used to compare SI *(a)* between the single RC and a pair of decoupled RCs and *(b)* between the RC and the vascular blood pool. Bland-Altman analysis was used to test for the limits of agreement between flow velocities measured next to the stent and in the lumen of the stent. Data for SI, stent position, and flow velocity were expressed as mean ± standard deviation. A value of $P < .05$ was considered to indicate a statistically significant difference. Interobserver variability for measurements of SI, stent position, and flow velocity was calculated by using the Bland-Altman test. Statistical analysis was performed by using software (Statistical Package for the Social Sciences, version 10.0 for Windows XP; SPSS, Chicago, Ill).

RESULTS

In Vitro Experiments

RCs produced an intense local signal enhancement, which clearly marked the margins of the stent loaded within the SDS (Fig 2). No significant difference in SI was measured between the single RCs and the pair of decoupled RCs when the SDS was aligned parallel to the B_0 field.

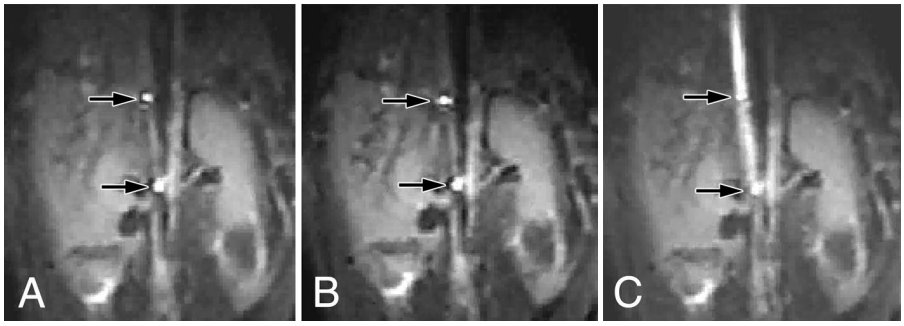

Figure 6. Transverse interactive steady-state free precession (2.9/1.6; flip angle, 45°; section thickness, 8 mm; acquisition frame rate, 8 per second; field of view, 280 mm; matrix, 128 × 128) MR images of the inferior vena cava and SDS with paired decoupled RCs (arrows) show that SI of the RCs remained comparable in three different conditions: with the working lumen of the SDS filled with saline solution (*A*); with a 0.035-inch polyester guidewire advanced through the saline solution–filled lumen (*B*); and with a 0.035-inch nitinol guidewire inserted in the saline solution–filled lumen (*C*). Because the nitinol guidewire acts as an antenna, SI in the SDS is increased on *C*.

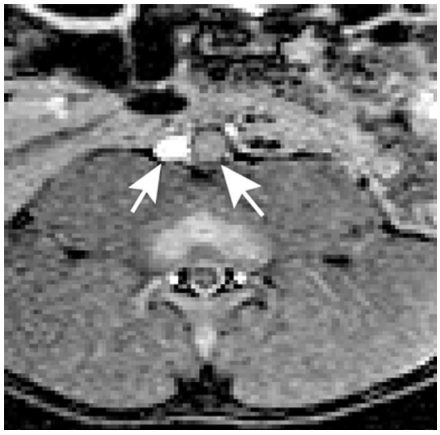

Figure 7. Transverse balanced FFE (2.7/1.4; flip angle, 50°; section thickness, 8 mm; field of view, 260 mm; matrix, 256 × 256) MR image shows decreased SI in the lumen of a nitinol stent placed in the aorta (right arrow), compared with SI in the adjacent vena cava (left arrow).

Mean SI of the single and paired RCs was 2744 arbitrary units (au) ± 97 and 2688 au ± 89, respectively. SI was orientation dependent for single RCs but not for the pair of decoupled RCs. In single RCs, SI decreased significantly ($P < .01$) when the SDS was positioned at an angle of more than 30° with respect to the B_0 field. The extent of the SI decrease depended on the rotation angle of the long axis of the catheter, which at a certain angulation resulted in total signal loss.

No significant difference in SI in either type of RC was noted between measurements made at a flip angle of 45° and those at a flip angle of 5°. In addition, SI levels measured before and after stent delivery were constant (Fig 2). During stent delivery, however, the distal RC was detuned as the outer catheter of the SDS was pulled, together with the distal RC, over the front-loaded stent. Detuning of the RC resulted in total signal loss. No significant difference in SI was measured between conditions in which the lumen of the SDS was *(a)* filled with saline solution, *(b)* filled with saline solution and containing a nitinol guidewire, or *(c)* filled with saline solution and containing a polyester guidewire. For the in vitro experiments, interobserver variability in measured SI was 1.3% ± 0.3.

In Vivo Experiments

During the interventional procedure, resonant markers produced an intense local MR signal (Figs 3, 4). For the observer, the signal was easy to distinguish from the background anatomy and allowed fast and reliable MR monitoring of the SDS position. The margins of the loaded stent were clearly and unequivocally defined by the RCs (Figs 3, 4). Stent placement was successful in all cases. There was no technical failure, stent malpositioning, or vascular injury due to the intervention. The SDS was maneuvered easily within the vasculature.

Mean SI of the pair of decoupled RCs was not substantially lower than mean SI of the single RCs (2381 au ± 123 and 2130 au ± 101, respectively) in the aorta and vena cava (Fig 5). SI levels of the pair of decoupled RCs were independent from the orientation of the SDS with respect to the B_0 field direction. SI levels of the single RCs remained constant when measured in the aorta and vena cava but decreased when the SDS was positioned at an angle with respect to the B_0 field. According to the results of in vitro experiments, SI decreased when the SDS was angled more than 30° with respect to the B_0 field (eg, when the SDS was moved through the aortic arch). The decrease in SI depended also on the rotation angle of the long axis of the RC, which at a certain angulation resulted in total signal loss. At angles greater than 30°, SI levels of single RCs ranged from 148 au (total signal loss) to 2360 au. Mean SI levels for the pair of decoupled RCs were 2145 au ± 121.

No significant difference in SI in RCs of either type was noted for measurements made at a flip angle of 45° or 5° (Fig 5). SI of the vascular space, however, decreased significantly from 1059 au ± 188 to 234 au ± 33 with a change in flip angle from 45° to 5° ($P < .001$), which, in turn, enhanced the contrast between the RC and the background anatomy (Figs 3–5).

No significant difference in SI of the RCs was found between measurement before and measurement after stent deployment. The distal part of the RC, however, detuned during stent delivery. Detuning resulted in total signal loss. No significant difference was found for the RC, whether the lumen of the SDS contained saline solution alone, saline solution and a nitinol guidewire, or saline solution and a polyester guidewire (Figs 5, 6). For the in vivo experiments, interobserver variability in measured SI was 1.8% ± 0.4.

After stent deployment, the position of the stent was verified on cine images acquired with the balanced FFE sequence and on 3D MR angiographic images (Figs 7, 8). The site of the deployed stent was evident because of magnetic susceptibility artifacts and radiofrequency shielding effects. All stents were successfully placed at the desired position. Stent position was confirmed at autopsy. Postmortem examination revealed that stents placed in the inferior vena cava or abdominal aorta were 3 mm ± 2 below the insertion of the renal veins or arteries and 2 mm ± 2 distal to the origin of the common carotid and iliac arteries from the aortic arch or aortic bifurcation. Interobserver variability of the determined stent position was 1.7% ± 0.4. The lumen of all placed stents was obscured because of radiofrequency shielding, which limited the evaluation of stent patency on balanced FFE and 3D MR angiographic images (Figs 7, 8). Assessment of blood flow velocity, however, was possible in all cases by using velocity-encoded cine MR imaging. The Bland-Altman test showed good agreement between peak flow velocities measured in the lumen of the stent

and those measured at locations distal or proximal to the stent. The mean difference was −9 cm/sec, and the standard deviation of difference was ± 5 cm/sec. All measurements were within the interval of two standard deviations. Stent patency was confirmed at autopsy. Interobserver variability of flow measurements was 2.3% ± 0.5.

DISCUSSION

The major finding of this study was that RCs provide an intense local MR signal in various major vessels and at various orientations that is easily perceived by the observer. At MR fluoroscopy, RCs clearly marked the position of the nitinol stent in the SDS. All stents were placed correctly in the desired sites shown on balanced FFE and 3D MR angiographic images. Postinterventional velocity-encoded cine MR imaging measurements of peak flow velocities indicated patency of the stent lumina, which was confirmed at autopsy.

In the current study, monitoring of the SDS position was based on visual perception of intense local SI enhancement in the area of the RCs. RCs, however, also have potential for automated tip detection and section tracking. Weiss et al (13) recently demonstrated that switchable RCs can be optically tuned and detuned with use of a photodiode connected to an optical fiber.

Orientation-independent position monitoring of catheters is essential to perform endovascular intervention safely. As previously reported by Kuehne et al (14), the MR signal of a pair of decoupled RCs is largely independent of catheter orientation with regard to the B_0 field. In this study, we mounted single RCs and a pair of decoupled RCs on the SDS. Unlike the pair of decoupled RCs, the single RCs were orientation dependent. Therefore, we used SDSs with single RCs for interventions in the aorta and vena cava and SDSs with a pair of decoupled RCs for interventions in the other blood vessels (eg, the carotid and iliac arteries), which are not strictly parallel to the B_0 field. Thus, a pair of decoupled RCs may be needed in tortuous blood vessels.

The use of guidewires in endovascular interventions with conventional fluoroscopic guidance is routine. Currently, research efforts have been undertaken to develop guidewires suitable for MR imaging–controlled intervention. In theory, the MR signal of RCs is very susceptible to changes induced by guidewires, metallic or not. Metallic guidewires can couple with the RC to produce a higher RC resonance frequency due to the reduction in the effective cross-sectional area of the coil and, thus, an increase in its inductance. In addition, the RC signal benefits from the signal that originates in the water in the lumen of the catheter. Thus, the insertion of any type of guidewire through the lumen of the catheter might cause a decrease in MR signal of the RC.

In this study, RCs were tuned when a 0.035-inch nitinol guidewire was placed in the lumen of the SDS. Removal of the guidewire slightly lowered the resonance frequency of RCs by 120 kHz ± 20. The results of in vitro and in vivo experiments, however, showed no significant difference between SI of the RCs measured during *(a)* use of a 0.035-inch nitinol guidewire, *(b)* use of a 0.035-inch polyester guidewire, and *(c)* retrieval of the guidewires (Fig 6). These findings can be explained by the fact that a shift in resonance frequency of 120 kHz is less than 15% of the RC bandwidth of approximately 1500 kHz when using an RC with a quality factor of 42. In addition, the coil configuration proposed in this article produces a very asymmetric magnetic field. Therefore, the generated RC signal certainly benefits from but does not necessarily depend on signal that originates in the lumen of the SDS.

In the current study, RCs were mounted on the outer catheter of the SDS and were positioned directly adjacent to the borders of the stent. During retraction of the outer catheter for stent delivery, the RC positioned at the distal tip of the SDS was pulled back and moved over the loaded stent. This caused severe detuning of the distal RC, which in turn resulted in total loss of the RC signal. This problem could be eventually solved by deploying RCs on the inner catheter of the SDS and not, as in this study, on the outer retractable sheath. Such a setup, however, has to be tested in a systematic manner in future research.

Real-time interactive steady-state free precession imaging allows interactive change of the flip angle, which can be helpful for fast monitoring of catheter position during MR imaging–guided intervention. Good visualization of the RCs and the background anatomy was realized at a flip angle of 45° (Fig 4). Small tortuous vessels with pulsatile blood flow may result, however, in circumscribed areas with high signal intensity that might appear similar to the signal intensity of RCs. In such cases, fast identification of the RCs can be facilitated with the use of a smaller flip angle (5°–10°). Use of small flip angles results in a substantial decrease in the SI of the background anatomy without a decrease in SI in the RCs. Consequently, the contrast between RCs and the anatomic background is much improved (Figs 3–5).

Balanced FFE and 3D MR angiographic imaging sequences were used for postinterventional assessment of stent position and patency. The combination of magnetic susceptibility artifacts and radiofrequency shielding effects allowed visualization of stents in the vascular beds. Radiofrequency shielding effects, however, also caused a reduction in SI in the lumen of the stent, which prevented a reliable assessment of patency in the stent lumen (Figs 7, 8). Nevertheless, we found, in concordance with the results of other studies, that quantitative blood

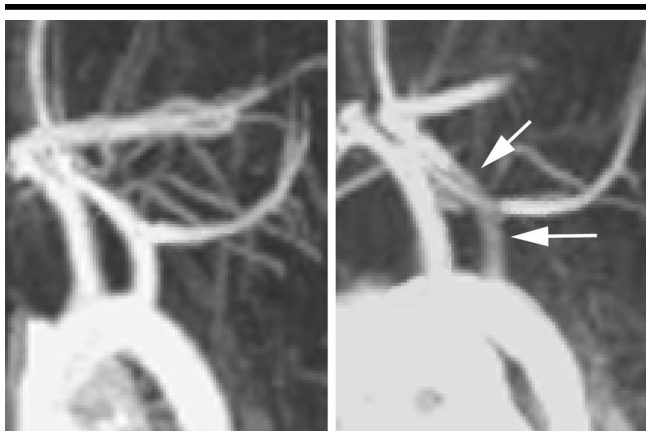

Figure 8. Contrast-enhanced MR angiograms (5.2/1.6; flip angle, 35°; section thickness, 1.6 mm; field of view, 380 mm; matrix, 512 × 512) before (left) and after (right) stent placement in the carotid artery (arrows).

flow rates can be accurately assessed within the lumen of nitinol stents with a diameter of 10 mm (17). Future research is required to determine whether postinterventional in-stent stenosis can be accurately determined by using velocity-encoded cine MR imaging.

The construction of very small RCs is time-consuming and technically difficult. Future research should address the development of techniques for producing smaller RCs. In addition, the potential use of RCs with small catheters (1–3 F) is questionable because the inductance of very small coils might be insufficient to produce any local enhancement of signal and hence SI. This matter should be investigated in a systematic manner.

In conclusion, the results of this study demonstrate that RCs are well suited for use in MR imaging–guided stent placement in the major blood vessels. Catheters with integrated RCs produce an intense local MR signal that is readily perceptible to the interventionist and allows variation of signal contrast between the RCs and the background anatomy with interactive adjustments of the flip angle. RCs can be used with interventional instruments such as guidewires and implant devices and may allow automated tip detection and section tracking in patients. Finally, MR imaging provides valuable information about the position of the stent immediately after placement and allows measurement of physiologic blood flow velocity within the lumen of nitinol stents.

Practical application: The use of RCs as fiducial markers of endovascular catheters during MR imaging–guided endovascular intervention has the potential to increase catheter tracking accuracy and enable avoidance of radiofrequency heating. The proposed MR imaging method could increase patient and operator safety.

Acknowledgment: We thank Maythem Saeed, DVM, PhD, Department of Radiology, University of California, San Francisco, for his friendly support.

References

1. Kuehne T, Saeed M, Higgins CB, et al. Endovascular stents in pulmonary valve and artery in swine: feasibility study of MR imaging-guided deployment and postinterventional assessment. Radiology 2003; 226:475–481.
2. Manke C, Nitz WR, Djavidani B, et al. MR imaging-guided stent placement in iliac arterial stenoses: a feasibility study. Radiology 2001; 219:527–534.
3. Spuentrup E, Ruebben A, Schaeffter T, Manning WJ, Gunther RW, Buecker A. Magnetic resonance–guided coronary artery stent placement in a swine model. Circulation 2002; 105:874–879.
4. Dumoulin CL, Souza SP, Darrow RD. Real-time position monitoring of invasive devices using magnetic resonance. Magn Reson Med 1993; 29:411–415.
5. Leung DA, Debatin JF, Wildermuth S, et al. Real-time biplanar needle tracking for interventional MR imaging procedures. Radiology 1995; 197:485–488.
6. Konings MK, Bartels LW, Smits HF, Bakker CJ. Heating around intravascular guidewires by resonating RF waves. J Magn Reson Imaging 2000; 12:79–85.
7. Ladd ME, Quick HH. Reduction of resonant RF heating in intravascular catheters using coaxial chokes. Magn Reson Med 2000; 43:615–619.
8. Liu CY, Farahani K, Lu DS, Duckwiler G, Oppelt A. Safety of MRI-guided endovascular guidewire applications. J Magn Reson Imaging 2000; 12:75–78.
9. Bakker CJ, Bos C, Weinmann HJ. Passive tracking of catheters and guidewires by contrast-enhanced MR fluoroscopy. Magn Reson Med 2001; 45:17–23.
10. Rubin DL, Ratner AV, Young SW. Magnetic susceptibility effects and their application in the development of new ferromagnetic catheters for magnetic resonance imaging. Invest Radiol 1990; 25:1325–1332.
11. Unal O, Korosec FR, Frayne R, Strother CM, Mistretta CA. A rapid 2D time-resolved variable-rate k-space sampling MR technique for passive catheter tracking during endovascular procedures. Magn Reson Med 1998; 40:356–362.
12. Weiss S, Schaeffter T, Luedeke KM, et al. Catheter localization using a resonant fiducial marker during interactive MR fluoroscopy (abstr). In: Proceedings of the Seventh Meeting of the International Society for Magnetic Resonance in Medicine. Berkeley, Calif: International Society for Magnetic Resonance in Medicine, 1999; 1954.
13. Weiss S, Schaeffter T, Brinkert F, Kuehne T, Buecker A. Approach for safe visualization and localization of catheters during MR-guided intravascular procedures. Z Med Phys 2003; 13:172–176. [German]
14. Kuehne T, Fahrig R, Butts K. Pair of resonant fiducial markers for localization of endovascular catheters at all catheter orientations. J Magn Reson Imaging 2003; 17:620–624.
15. Schenck JF. The role of magnetic susceptibility in magnetic resonance imaging: MRI magnetic compatibility of the first and second kinds. Med Phys 1996; 23: 815–850.
16. Kuehne T, Saeed M, Reddy G, et al. Sequential magnetic resonance monitoring of pulmonary flow with endovascular stents placed across the pulmonary valve in growing swine. Circulation 2001; 104: 2363–2368.
17. van Holten J, Kunz P, Mulder PG, Pattynama PM, Lamb HJ, van Dijk LC. MR-velocity mapping in vascular stents to assess peak systolic velocity: in vitro comparison of various stent designs made of stainless steel and nitinol. MAGMA 2002; 15:52–57.